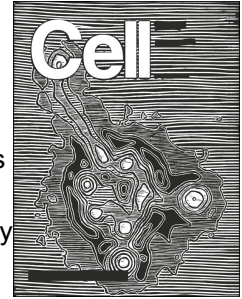


# Journal Pre-proof



Alarming antibody evasion properties of rising SARS-CoV-2 BQ and XBB subvariants

Qian Wang, Sho Iketani, Zhiteng Li, Liyuan Liu, Yicheng Guo, Yiming Huang, Anthony D. Bowen, Michael Liu, Maple Wang, Jian Yu, Riccardo Valdez, Adam S. Luring, Zizhang Sheng, Harris H. Wang, Aubree Gordon, Lihong Liu, David D. Ho

PII: S0092-8674(22)01531-8

DOI: <https://doi.org/10.1016/j.cell.2022.12.018>

Reference: CELL 12736

To appear in: *Cell*

Received Date: 21 November 2022

Revised Date: 5 December 2022

Accepted Date: 8 December 2022

Please cite this article as: Wang, Q., Iketani, S., Li, Z., Liu, L., Guo, Y., Huang, Y., Bowen, A.D., Liu, M., Wang, M., Yu, J., Valdez, R., Luring, A.S., Sheng, Z., Wang, H.H., Gordon, A., Liu, L., Ho, D.D., Alarming antibody evasion properties of rising SARS-CoV-2 BQ and XBB subvariants *Cell* (2023), doi: <https://doi.org/10.1016/j.cell.2022.12.018>.

This is a PDF file of an article that has undergone enhancements after acceptance, such as the addition of a cover page and metadata, and formatting for readability, but it is not yet the definitive version of record. This version will undergo additional copyediting, typesetting and review before it is published in its final form, but we are providing this version to give early visibility of the article. Please note that, during the production process, errors may be discovered which could affect the content, and all legal disclaimers that apply to the journal pertain.

© 2022 The Author(s). Published by Elsevier Inc.



## Alarming antibody evasion properties of rising SARS-CoV-2

### BQ and XBB subvariants

Qian Wang<sup>1,8</sup>, Sho Iketani<sup>1,8</sup>, Zhiteng Li<sup>1,8</sup>, Liyuan Liu<sup>2,8</sup>, Yicheng Guo<sup>1,8</sup>, Yiming Huang<sup>2</sup>, Anthony D. Bowen<sup>1,3</sup>, Michael Liu<sup>1</sup>, Maple Wang<sup>1</sup>, Jian Yu<sup>1</sup>, Riccardo Valdez<sup>4</sup>, Adam S. Lauring<sup>5</sup>, Zizhang Sheng<sup>1</sup>, Harris H. Wang<sup>2</sup>, Aubree Gordon<sup>4</sup>, Lihong Liu<sup>1\*</sup>, and David D. Ho<sup>1,3,6,7\*</sup>

<sup>1</sup>Aaron Diamond AIDS Research Center, Columbia University Vagelos College of Physicians and Surgeons, New York, NY, USA.

<sup>2</sup>Department of Systems Biology, Columbia University Vagelos College of Physicians and Surgeons, New York, NY, USA.

<sup>3</sup>Division of Infectious Diseases, Department of Medicine, Columbia University Vagelos College of Physicians and Surgeons, New York, NY, USA.

<sup>4</sup>Department of Epidemiology, University of Michigan, Ann Arbor, MI, USA.

<sup>5</sup>Division of Infectious Diseases, Department of Internal Medicine, University of Michigan, Ann Arbor, MI, USA.

<sup>6</sup>Department of Microbiology and Immunology, Columbia University Vagelos College of Physicians and Surgeons, New York, NY, USA.

<sup>7</sup>Lead contact

<sup>8</sup>These authors contributed equally

\*Correspondence: [ll3411@cumc.columbia.edu](mailto:ll3411@cumc.columbia.edu) (Lihong. L.), [dh2994@cumc.columbia.edu](mailto:dh2994@cumc.columbia.edu) (D.D.H.)

**1 SUMMARY**

2 The BQ and XBB subvariants of SARS-CoV-2 Omicron are now rapidly expanding, possibly due  
3 to altered antibody evasion properties deriving from their additional spike mutations. Here, we  
4 report that neutralization of BQ.1, BQ.1.1, XBB, and XBB.1 by sera from vaccinees and infected  
5 persons was markedly impaired, including sera from individuals boosted with a WA1/BA.5  
6 bivalent mRNA vaccine. Titers against BQ and XBB subvariants were lower by 13-81-fold and  
7 66-155-fold, respectively, far beyond what had been observed to date. Monoclonal antibodies  
8 capable of neutralizing the original Omicron variant were largely inactive against these new  
9 subvariants, and the responsible individual spike mutations were identified. These subvariants  
10 were found to have similar ACE2-binding affinities as their predecessors. Together, our findings  
11 indicate that BQ and XBB subvariants present serious threats to current COVID-19 vaccines,  
12 render inactive all authorized antibodies, and may have gained dominance in the population  
13 because of their advantage in evading antibodies.

14  
15 **Keywords:** SARS-CoV-2, BQ.1, BQ.1.1, XBB, XBB.1, COVID-19, neutralizing monoclonal  
16 antibody, mRNA vaccine, receptor binding affinity, antibody evasion

## 17 INTRODUCTION

18 The coronavirus disease 2019 (COVID-19) pandemic, caused by severe acute respiratory  
19 syndrome coronavirus 2 (SARS-CoV-2), continues to rage due to emergence of the Omicron  
20 variant and its descendant subvariants.<sup>1-5</sup> While the BA.5 subvariant is globally dominant at this  
21 time (**Figure 1A**), a diverse array of Omicron sublineages have arisen and are competing in the  
22 so-called “variant soup”.<sup>6</sup> It has become apparent that four new subvariants are rapidly gaining  
23 ground on BA.5, raising the specter of yet another wave of infections in the coming months. BQ.1  
24 and BQ.1.1 were first identified in Nigeria in early July and then expanded dramatically in Europe  
25 and North America, now accounting for 67%, 35%, and 47% of cases in France, the United  
26 Kingdom, and the United States, respectively (**Figure 1A**). XBB and XBB.1 were first identified  
27 in India in mid-August and quickly became predominant in India, Singapore, and other regions in  
28 Asia (**Figure 1A**). BQ.1 and BQ.1.1 evolved from BA.5, whereas XBB and XBB.1 resulted from  
29 a recombination between two BA.2 lineages, BJ.1 and BA.2.75 (**Figure 1B**). These two  
30 sublineages are continuing to evolve and diversify, with an ever increasing complexity of spike  
31 mutations. However, the spike protein of the predominant BQ.1 subvariant harbors the K444T  
32 and N460K mutations in addition to those found in BA.5, with BQ.1.1 having an additional R346T  
33 mutation (**Figures 1C and S1**). Strikingly, the spike of the predominant XBB subvariant has 14  
34 mutations in addition to those found in BA.2, including 5 in the N-terminal domain (NTD) and 9  
35 in the receptor-binding domain (RBD), whereas XBB.1 has an additional G252V mutation  
36 (**Figures 1C and S1**). The rapid rise of these subvariants and their extensive array of spike  
37 mutations are reminiscent of the appearance of the first Omicron variant last year, thus raising  
38 concerns that they may further compromise the efficacy of current COVID-19 vaccines and  
39 monoclonal antibody therapeutics. We now report findings that indicate that such concerns are,  
40 sadly, justified, especially so for the XBB and XBB.1 subvariants.

41

## 42 RESULTS

### 43 Neutralization by polyclonal sera

44 To understand if BQ.1, BQ.1.1, XBB, and XBB.1 have stronger resistance to serum antibodies,  
45 we first set out to evaluate the neutralization of these four new subvariants by sera from five  
46 different clinical cohorts. These results are summarized in **Figure 2**. The five clinical cohorts  
47 included individuals who received three or four doses of one of the original COVID-19 mRNA

48 vaccines (termed “3 shots WT” or “4 shots WT”, respectively), those who received one of the  
49 recently authorized bivalent (WT and BA.5) COVID-19 mRNA vaccines as a 4<sup>th</sup> shot after three  
50 doses of one of the original COVID-19 mRNA vaccines (termed “3 shots WT + bivalent”), and  
51 patients who had BA.2 and BA.4 or BA.5 breakthrough infection after vaccination (termed “BA.2  
52 breakthrough” and “BA.4/5 breakthrough”, respectively). Their relevant clinical information is  
53 summarized in **Table S1**. Consistent with previous findings<sup>2</sup>, BA.2 and BA.4/5 showed stronger  
54 evasion to serum neutralization relative to the ancestral strain D614G across all five cohorts  
55 (**Figure 2A**). The geometric mean 50% inhibitory dose (ID<sub>50</sub>) titers against BA.2 and BA.4/5  
56 decreased 2.9- to 7.8-fold and 3.7- to 14-fold, respectively, compared to that against D614G.  
57 Alarming, in the “3 shots WT” cohort, neutralization titers were far lower against BQ.1, BQ.1.1,  
58 XBB, and XBB.1, with reductions of >37-fold to >71-fold compared to D614G. Moreover, while  
59 all sera had detectable titers against BA.2 and BA.4/5, a majority of samples did not neutralize the  
60 new subvariants at the lowest dilution (1:100) of serum tested. A similar trend was also noted in  
61 the other four cohorts, with the lowest titers observed against XBB.1, followed by XBB, BQ.1.1,  
62 and BQ.1. The geometric mean neutralization titers of sera from the “BA.4/5 breakthrough” and  
63 “BA.2 breakthrough” cohorts were noticeably higher, indicating that SARS-CoV-2 breakthrough  
64 infection induced better antibody responses than vaccination among these samples.

65  
66 We then utilized the serum neutralization results to construct an antigenic map to depict the  
67 antigenic distances among D614G and the Omicron subvariants<sup>2</sup> (**Figure 2B**). The resulting map  
68 shows that BQ.1.1 has drifted away from BA.4/5 antigenically as much as the latter has from the  
69 ancestral D614G. With each antigenic unit equaling a 2-fold difference in virus neutralization,  
70 BQ.1.1 is approximately 6-fold more resistant to serum neutralization than its predecessor BA.5.  
71 On the other hand, it is clear that XBB.1 is the most antigenically distinct of the Omicron  
72 subvariants. The large number of antigenic units that separates XBB.1 and BA.2 suggests that this  
73 new subvariant is ~63-fold more resistant to serum neutralization than its predecessor, or ~49-fold  
74 more resistant than BA.4/5. The impact of this antigenic shift on vaccine efficacy is particularly  
75 concerning.

76

77 **Neutralization by monoclonal antibodies**

78 To understand the types of serum antibodies that lost neutralizing activity against BQ.1, BQ.1.1,  
79 XBB, and XBB.1, we constructed pseudoviruses for each subvariant, as well as for each individual  
80 mutation found in the subvariants, and then evaluated their susceptibility to neutralization by a  
81 panel of 23 monoclonal antibodies (mAbs) targeting various epitopes on the spike (**Figure 3A**).  
82 These mAbs were chosen because they had appreciable activity against the initial Omicron variant.  
83 Among these antibodies, 20 were directed to the class 1 to class 4 epitope clusters on the RBD<sup>8</sup>:  
84 S2K146<sup>9</sup>, Omi-3<sup>10</sup>, Omi-18<sup>10</sup>, BD-515<sup>11</sup>, XGv051<sup>12</sup>, XGv347<sup>13</sup>, ZCB11<sup>14</sup>, COV2-2196  
85 (tixagevimab)<sup>15</sup>, LY-CoV1404 (bebtelovimab, authorized to treat COVID-19)<sup>16</sup>, XGv289<sup>13</sup>,  
86 XGv264<sup>12</sup>, S309 (sotrovimab)<sup>17</sup>, P2G3<sup>18</sup>, SP1-77<sup>19</sup>, BD55-5840<sup>20</sup>, XGv282<sup>13</sup>, BD-804<sup>21</sup>, 35B5<sup>22</sup>,  
87 COV2-2130 (cilgavimab)<sup>15</sup>, and 10-40<sup>23</sup>. The other three were non-RBD mAbs, with C1520<sup>24</sup>  
88 targeting the NTD, C1717<sup>24</sup> targeting NTD-SD2, and S3H3<sup>25</sup> targeting SD1. We also included  
89 the clinical mAb combination of COV2-2196 and COV2-2130, marketed as Evusheld for the  
90 prevention of SARS-CoV-2 infection. Their neutralization IC<sub>50</sub> values are presented in the **Figure**  
91 **S2** and their fold changes in IC<sub>50</sub> compared to BA.4/5 or BA.2 are shown in **Figure 3B**. BQ.1 and  
92 BQ.1.1 were greatly or completely resistant to all RBD class 1 and class 3 mAbs tested as well as  
93 to one RBD class 2 mAb (XGv051), a class 4 mAb (10-40), and an NTD-SD2 mAb (C1717). The  
94 loss of neutralizing activity of NTD-SD2 and RBD class 1 mAbs were due to the N460K mutation,  
95 while the impairment in the potency of RBD class 3 mAbs resulted from both the R346T and  
96 K444T mutations. As BQ.1.1 has one more mutation (R346T) than BQ.1, it exhibited stronger  
97 antibody evasion to the class 3 RBD mAbs than BQ.1. It is also noteworthy that BQ.1.1, XBB,  
98 and XBB.1 share R346T and N460K, showing evolutionary convergence to avoiding antibodies  
99 directed to these spike regions. Importantly, clinically authorized LY-CoV1404 (bebtelovimab)  
100 and Evusheld were inactive against BQ.1 or BQ.1.1.

101  
102 Against XBB and XBB.1, 19 of 23 mAbs lost neutralizing activity greatly or completely. Only  
103 C1717, S3H3, S309 (sotrovimab), and 10-40 showed relatively little fold change in neutralizing  
104 activity against these two subvariants relative to BA.2, although we note that these mAbs, with the  
105 exception of S3H3, had already lost significant activity against BA.2 relative to D614G (**Figure**  
106 **S2**). The Q183E mutation contributed to the activity loss of C1520; N460K and F486S accounted  
107 for the resistance to the RBD class 1 and class 2 mAbs; and R346T, V455P, G446S, and F490S

108 contributed to the resistance to the RBD class 3 mAbs. Again, the clinically authorized LY-  
109 CoV1404 (bebtelovimab) and Evusheld could not neutralize XBB or XBB.1.

110  
111 Several aforementioned point mutants (R346T, N460K, and F486S) had been observed in prior  
112 SARS-CoV-2 variants, and their impact on mAb binding have been reported.<sup>2,4,5</sup> We therefore  
113 conducted structural modeling to understand the impact of the newly identified point mutants  
114 (Q183E, K444T, V445P, and F490S) on the binding of select mAbs (**Figure 4**). The Q183E  
115 mutation in XBB and XBB.1 disrupted the hydrogen bond that residue A32 of mAb C1520 has  
116 with the spike and caused a steric clash with residue W91, likely abrogating the binding of this  
117 mAb (**Figure 4A**). K444T, found in BQ.1 and BQ.1.1, impaired the neutralization activities of  
118 most of the class 3 mAbs tested (**Figure 3B**), probably because mutating lysine to threonine made  
119 the side chain shorter and uncharged, which in turn would impair the interactions of this residue  
120 with mAbs directed to this site, as can be seen with SP1-77 and LY-CoV1404 (**Figures 4B and**  
121 **4C**). Similarly, the V445P substitution in XBB and XBB.1 could exert an equivalent effect as  
122 K444T, by causing steric hindrance and/or disrupting a hydrogen bond with mAbs, resulting in the  
123 loss of antibody neutralization (**Figures 4D and 4E**). Finally, F490S impaired the neutralizing  
124 activities of XGv282, which can be accounted for by the abolition of a cation- $\pi$  interaction (**Figure**  
125 **4F**).

126

### 127 **Receptor affinity**

128 Angiotensin converting enzyme 2 (ACE2) is the receptor responsible for the entry of SARS-CoV-  
129 2 into target cells, and the binding affinity for this receptor may influence the transmissibility of  
130 the virus. We generated the spike trimer proteins of BA.2, BA.4/5, BQ.1, BQ.1.1, XBB, and  
131 XBB.1, and then tested their binding affinities to human ACE2 (hACE2) using surface plasmon  
132 resonance (SPR) (**Figure 5**). Our results showed that the viral receptor affinities of BQ.1 and  
133 BQ.1.1 spikes were comparable to that of BA.4/5 spike, with  $K_D$  ranging from 0.56 nM to 0.62  
134 nM. The binding affinities for hACE2 of XBB and XBB.1 spikes exhibited a modest drop relative  
135 to that of BA.2 spike ( $K_D$  of 2.00 nM and 2.06 nM versus 0.95 nM). These findings suggested that  
136 the combination of mutations found in BQ.1 and BQ.1.1 did not alter the spike binding affinity to  
137 hACE2. The modest loss in hACE2 affinity for XBB and XBB.1 spikes may be due to F486S and  
138 R493Q mutations, which reside at the top of the RBD, where similar mutations, F486V and R493Q,



139 were previously observed in BA.4/5 to impair and improve hACE2 binding, respectively.<sup>2</sup> In XBB  
140 and XBB.1, the serine rather than a valine may lower hACE2 binding, as has been observed in a  
141 deep mutational scanning study<sup>26</sup>. Overall, these SPR measurements provide no evidence that the  
142 rise of these new subvariants is due to a higher affinity for hACE2.

143

## 144 **DISCUSSION**

145 In summary, we have examined in detail the antibody resistance profile and viral receptor binding  
146 affinity of SARS-CoV-2 Omicron BQ.1, BQ.1.1, XBB, and XBB.1 subvariants, which are rapidly  
147 expanding globally and already predominant regionally (**Figure 1A**). Our data demonstrate that  
148 these new subvariants were barely susceptible to neutralization by sera from vaccinated individuals  
149 with or without prior infection, including persons recently boosted with the new bivalent (WA1-  
150 BA.5) mRNA vaccines (**Figure 2**). The extent of the antigenic drift or shift measured herein is  
151 comparable to the antigenic leap made by the initial Omicron variant from its predecessors one  
152 year ago. In fact, combining these results with our prior findings on the serum neutralization of  
153 select sarbecoviruses<sup>27</sup>, there are indications that XBB and XBB.1 are now antigenically more  
154 distant than SARS-CoV or some sarbecoviruses in animals (**Figure S3**). Therefore, it is alarming  
155 that these newly emerged subvariants could further compromise the efficacy of current COVID-  
156 19 vaccines and result in a surge of breakthrough infections, as well as re-infections. However, it  
157 is important to emphasize that although infections may now be more likely, COVID-19 vaccines  
158 have been shown to remain effective at preventing hospitalization and severe disease even against  
159 Omicron<sup>28-31</sup> as well as possibly reducing the risk of post-acute sequelae of COVID-19 (PASC or  
160 long COVID)<sup>32-34</sup>.

161

162 We also showed that these new subvariants were completely or partially resistant to neutralization  
163 by most monoclonal antibodies tested, including those with Emergency Use Authorization  
164 (**Figures 3B and S2**). These findings helped to define the causes behind the loss of serum  
165 neutralizing activity. BQ.1 and BQ.1.1 are largely pan-resistant to antibodies targeting the RBD  
166 class 1 and class 3 epitopes, whereas XBB and XBB.1 are pan-resistant to antibodies targeting the  
167 RBD class 1, 2, and 3 epitopes. These BQ and XBB sublineages have evolved additional mutations  
168 that are seemingly “filling up the holes” that allow a few mAbs to get through and neutralize their

169 Omicron predecessors. Interestingly, both sublineages have converged on identical (R346T and  
170 N460K) or similar solutions (K444T versus V445P and G446S) to enhance antibody evasion.  
171 Furthermore, we have provided structural explanations for antibody resistance of various point  
172 mutants, including three that were previously undescribed (Q183E, K444T, and V445P) (**Figure**  
173 **4**).

174  
175 Perhaps the most important outcome of these mAb studies is the clinical implication for the use of  
176 mAbs to treat or prevent COVID-19. Previous SARS-CoV-2 variants have already successively  
177 knocked out the use of clinically authorized therapeutic antibodies (bamlanivimab, etesevimab,  
178 imdevimab, casirivimab, tixagevimab, cilgavimab, and sotrovimab), with bebtelovimab remaining  
179 as the only active monoclonal antibody against circulating SARS-CoV-2 strains<sup>1-5,35</sup>.  
180 Unfortunately, both BQ and XBB sublineages are now completely resistant to bebtelovimab,  
181 leaving us with no authorized antibody for treatment use. In addition, the combination of mAbs  
182 known as Evusheld that is authorized for the prevention of COVID-19 is also completely inactive  
183 against the new subvariants. This poses a serious problem for millions of immunocompromised  
184 individuals who do not respond robustly to COVID-19 vaccines. The urgent need to develop  
185 active monoclonal antibodies for clinical use is obvious.

186  
187 Lastly, we found that the spikes of BQ and XBB subvariants have similar binding affinities to  
188 hACE2 as the spikes of their predecessors (**Figure 5**), suggesting that the recently observed growth  
189 advantage for these novel subvariants is likely due to some other factors. Foremost may be their  
190 extreme antibody evasion properties, especially considering the extensive herd immunity built up  
191 in the population over the last three years from infections and vaccinations. BQ.1, BQ.1.1, XBB,  
192 and XBB.1 subvariants exhibit far greater antibody resistance than earlier variants, and they may  
193 fuel yet another surge of COVID-19 infections. We have collectively chased after SARS-CoV-2  
194 variants for over two years, and yet, the virus continues to evolve and evade. This continuing  
195 challenge highlights the importance of developing vaccine and monoclonal antibody approaches  
196 that protect broadly and anticipate the antigenic trajectory of SARS-CoV-2.

197

198 **Limitations of the Study**

199 The work presented herein have all been conducted *in vitro*, and while such studies for SARS-  
200 CoV-2 have been largely predictive of *in vivo* outcomes, efficacy of COVID-19 vaccines against  
201 BQ and XBB sublineages will need to be assessed in clinical studies. In addition, we have not  
202 studied cellular immunity to these new subvariants, which would be expected to play a role in  
203 vaccine efficacy.

Journal Pre-proof

204 **FIGURE LEGENDS**

205 **Figure 1 The rise of SARS-CoV-2 Omicron BQ.1, BQ.1.1, XBB, and XBB.1 subvariants.**

206 (A) Frequencies of Omicron subvariants from the GISAID. Variants were designated according to  
 207 their Pango dynamic lineage classification<sup>26</sup>. Minor sublineages of each subvariant were  
 208 grouped together with their parental variant. The values in the upper left corner of each box  
 209 denotes the cumulative number of sequences for all circulating viruses in the denoted time  
 210 period.

211 (B) Unrooted phylogenetic tree of Omicron subvariants along with other main SARS-CoV-2  
 212 variants. The scale bar indicates the genetic distance.

213 (C) Key spike mutations found in XBB and XBB.1 in the background of BA.2 and in BQ.1 and  
 214 BQ.1.1 in the background of BA.4/5. Del, deletion. The positions of these mutations on the  
 215 spike trimer are shown in **Figure S1**.

216

217 **Figure 2 Serum neutralization of Omicron subvariants BQ.1, BQ.1.1, XBB, and XBB.1.**

218 (A) Neutralization of pseudotyped D614G and Omicron subvariants by sera from five different  
 219 clinical cohorts, with their clinical information summarized in Table S1. The limit of detection  
 220 is 100 (dotted line). Values above the symbols denote the geometric mean ID<sub>50</sub> values, and  
 221 values beneath the symbols denote the numbers of samples that lost neutralization activity.  
 222 Values on the lower left show the sample size (*n*) for each group. The fold reduction in  
 223 geometric mean ID<sub>50</sub> value for each variant compared to D614G is also shown above the  
 224 symbols. Comparisons were made by two-tailed Wilcoxon matched-pairs signed-rank tests.  
 225 \*\*\**p* < 0.001; \*\*\*\**p* < 0.0001.

226 (B) Antigenic map based on the serum neutralization data from (A). Virus positions are represented  
 227 by closed circles while serum positions are shown as open squares. Sera are colored by group.  
 228 Both axes represent antigenic distance with one antigenic distance unit (AU) in any direction  
 229 corresponding to a two-fold change in neutralization ID<sub>50</sub> titer.

230 See also **Table S1 and Figure S3**.

231

232 **Figure 3 Resistance of Omicron subvariants to monoclonal antibody neutralization.**

233 (A) Footprints of NTD- and RBD-directed antibodies tested are outlined, and mutations within  
 234 BQ.1, BQ.1.1, XBB, and XBB.1 are highlighted in red.

235 (B) The fold changes in neutralization  $IC_{50}$  values of BQ.1, BQ.1.1, XBB, XBB.1, and the  
236 individual mutants compared with BA.4/5 or BA.2, with resistance colored red and  
237 sensitization colored green. The raw  $IC_{50}$  values are shown in **Figure S2**.

238 **Figure 4 Structural analysis of mutational effects on binding of mAbs.** Modeling of how (A)  
239 Q183E affects mAb C1520 neutralization, and how (B, C) K444T, (D, E) V445P, and (F) F490S  
240 affect RBD class 3 mAbs. Interactions are shown as yellow dotted lines and clashes are indicated  
241 as red asterisks.

242

243 **Figure 5 Receptor binding affinities of Omicron subvariant spikes.** Each spike was produced  
244 and purified as prefusion-stabilized trimers, and their binding to human ACE2 was measured by  
245 SPR.

246

247

#### 248 SUPPLEMENTAL INFORMATION

249 **Figure S1** Key mutations of BQ.1 and BQ.1.1 in the context of BA.4/5 (**a**), and key mutations of  
250 XBB and XBB.1 in the context of BA.2 (**b**).

251 See also **Figure 1**.

252

253 **Figure S2** Pseudovirus neutralization  $IC_{50}$  values for mAbs against D614G, Omicron subvariants,  
254 and point mutants of BQ.1, BQ.1.1, XBB, and XBB.1 in the background of BA.4/5 or BA.2.

255 See also **Figure 3**.

256

257 **Figure S3** Antigenic map of BQ.1, BQ.1.1, XBB, and XBB.1 in relation to sarbecoviruses.

258 See also **Figure 2**.

259

260 **Table S1** Demographics of the clinical cohorts.

261 See also **Figure 2**.

**262 STAR METHODS****263 Key resource table****264 Resource availability**

- 265 • Lead contact
- 266 • Materials availability
- 267 • Data and code availability

**268 Experimental model and subjects**

- 269 • Human subjects
- 270 • Cell lines

**271 Method details**

- 272 • Monoclonal antibodies
- 273 • Variant SARS-CoV-2 spike plasmid construction
- 274 • Protein expression and purification
- 275 • Surface plasmon resonance (SPR)
- 276 • Pseudovirus production
- 277 • Pseudovirus neutralization assay
- 278 • Antibody footprint and mutagenesis analysis
- 279 • Antigenic cartography

280

**281 QUANTIFICATION AND STATISTICAL ANALYSIS**

282

**283 ACKNOWLEDGEMENTS**

284 This study was supported by funding from the NIH SARS-CoV-2 Assessment of Viral Evolution  
285 (SAVE) Program and through the National Institutes of Health Collaborative Influenza Vaccine  
286 Innovation Center (75N93019C00051). We acknowledge Michael T. Yin and Magdalena E.  
287 Sobieszczyk for providing serum samples. We thank all who contributed their data to GISAID.

288

**289 AUTHOR CONTRIBUTIONS**

290 D.D.H. and Lihong L. conceived this project. Q.W., S.I., Z.L., and Lihong L. conducted  
291 pseudovirus neutralization assays and purified SARS-CoV-2 spike proteins. Y.G. and Z.S.  
292 conducted bioinformatic analyses. Q.W., Liyuan L., Y.H., H.H.W., and Lihong L. constructed the

293 spike expression plasmids. Q.W. managed the project. J.Y. M.W., and M.L. expressed and  
294 purified antibodies. Z.L. performed SPR assay and structural analyses. R.V., A.L., and A.G.  
295 provided clinical samples. A.B. generated antigenic map. D.D.H. and Lihong.L. directed and  
296 supervised the project. Q.W., S.I., Z.L., Y.G., A.B., Lihong L., and D.D.H. analyzed the results  
297 and wrote the manuscript.

298

#### 299 **DECLARATION OF INTERESTS**

300 S.I, J.Y., Lihong.L., and D.D.H. are inventors on patent applications (WO2021236998) or  
301 provisional patent applications (63/271,627) filed by Columbia University for a number of SARS-  
302 CoV-2 neutralizing antibodies described in this manuscript. Both sets of applications are under  
303 review. D.D.H. is a co-founder of TaiMed Biologics and RenBio, consultant to WuXi Biologics  
304 and Brie Biosciences, and board director for Vicarious Surgical. Aubree Gordon serves on a  
305 scientific advisory board for Janssen Pharmaceuticals. Other authors declare no competing  
306 interests.

307

## 308 REFERENCES

- 309 1. Liu, L., Iketani, S., Guo, Y., Chan, J.F., Wang, M., Liu, L., Luo, Y., Chu, H., Huang, Y., Nair, M.S., et al.  
 310 (2022). Striking antibody evasion manifested by the Omicron variant of SARS-CoV-2. *Nature* *602*,  
 311 676-681. 10.1038/s41586-021-04388-0.
- 312 2. Wang, Q., Guo, Y., Iketani, S., Nair, M.S., Li, Z., Mohri, H., Wang, M., Yu, J., Bowen, A.D., Chang, J.Y.,  
 313 et al. (2022). Antibody evasion by SARS-CoV-2 Omicron subvariants BA.2.12.1, BA.4, & BA.5. *Nature*.  
 314 10.1038/s41586-022-05053-w.
- 315 3. Iketani, S., Liu, L., Guo, Y., Liu, L., Chan, J.F., Huang, Y., Wang, M., Luo, Y., Yu, J., Chu, H., et al.  
 316 (2022). Antibody evasion properties of SARS-CoV-2 Omicron sublineages. *Nature* *604*, 553-556.  
 317 10.1038/s41586-022-04594-4.
- 318 4. Wang, Q., Iketani, S., Li, Z., Guo, Y., Yeh, A.Y., Liu, M., Yu, J., Sheng, Z., Huang, Y., Liu, L., and Ho, D.D.  
 319 (2022). Antigenic characterization of the SARS-CoV-2 Omicron subvariant BA.2.75. *Cell Host*  
 320 *Microbe*. 10.1016/j.chom.2022.09.002.
- 321 5. Wang, Q., Li, Z., Ho, J., Guo, Y., Yeh, A.Y., Mohri, H., Liu, M., Wang, M., Yu, J., Shah, J.G., et al.  
 322 (2022). Resistance of SARS-CoV-2 omicron subvariant BA.4.6 to antibody neutralisation. *Lancet*  
 323 *Infect Dis*. 10.1016/S1473-3099(22)00694-6.
- 324 6. Callaway, E. (2022). COVID 'variant soup' is making winter surges hard to predict. *Nature*.  
 325 10.1038/d41586-022-03445-6.
- 326 7. Smith, D.J., Lapedes, A.S., de Jong, J.C., Bestebroer, T.M., Rimmelzwaan, G.F., Osterhaus, A.D., and  
 327 Fouchier, R.A. (2004). Mapping the antigenic and genetic evolution of influenza virus. *Science* *305*,  
 328 371-376. 10.1126/science.1097211.
- 329 8. Barnes, C.O., Jette, C.A., Abernathy, M.E., Dam, K.A., Esswein, S.R., Gristick, H.B., Malyutin, A.G.,  
 330 Sharaf, N.G., Huey-Tubman, K.E., Lee, Y.E., et al. (2020). SARS-CoV-2 neutralizing antibody  
 331 structures inform therapeutic strategies. *Nature* *588*, 682-687. 10.1038/s41586-020-2852-1.
- 332 9. Park, Y.J., De Marco, A., Starr, T.N., Liu, Z., Pinto, D., Walls, A.C., Zatta, F., Zepeda, S.K., Bowen, J.E.,  
 333 Sprouse, K.R., et al. (2022). Antibody-mediated broad sarbecovirus neutralization through ACE2  
 334 molecular mimicry. *Science* *375*, 449-454. 10.1126/science.abm8143.
- 335 10. Nutalai, R., Zhou, D., Tuekprakhon, A., Ginn, H.M., Supasa, P., Liu, C., Huo, J., Mentzer, A.J.,  
 336 Duyvesteyn, H.M.E., Djikaite-Guraliuc, A., et al. (2022). Potent cross-reactive antibodies following  
 337 Omicron breakthrough in vaccinees. *Cell* *185*, 2116-2131 e2118. 10.1016/j.cell.2022.05.014.
- 338 11. Cao, Y., Yisimayi, A., Bai, Y., Huang, W., Li, X., Zhang, Z., Yuan, T., An, R., Wang, J., Xiao, T., et al.  
 339 (2021). Humoral immune response to circulating SARS-CoV-2 variants elicited by inactivated and  
 340 RBD-subunit vaccines. *Cell Res* *31*, 732-741. 10.1038/s41422-021-00514-9.
- 341 12. Wang, L., Fu, W., Bao, L., Jia, Z., Zhang, Y., Zhou, Y., Wu, W., Wu, J., Zhang, Q., Gao, Y., et al. (2022).  
 342 Selection and structural bases of potent broadly neutralizing antibodies from 3-dose vaccinees that  
 343 are highly effective against diverse SARS-CoV-2 variants, including Omicron sublineages. *Cell Res* *32*,  
 344 691-694. 10.1038/s41422-022-00677-z.
- 345 13. Wang, K., Jia, Z., Bao, L., Wang, L., Cao, L., Chi, H., Hu, Y., Li, Q., Zhou, Y., Jiang, Y., et al. (2022).  
 346 Memory B cell repertoire from triple vaccinees against diverse SARS-CoV-2 variants. *Nature* *603*,  
 347 919-925. 10.1038/s41586-022-04466-x.
- 348 14. Zhou, B., Zhou, R., Tang, B., Chan, J.F., Luo, M., Peng, Q., Yuan, S., Liu, H., Mok, B.W., Chen, B., et al.  
 349 (2022). A broadly neutralizing antibody protects Syrian hamsters against SARS-CoV-2 Omicron  
 350 challenge. *Nat Commun* *13*, 3589. 10.1038/s41467-022-31259-7.
- 351 15. Zost, S.J., Gilchuk, P., Case, J.B., Binshtein, E., Chen, R.E., Nkolola, J.P., Schafer, A., Reidy, J.X.,  
 352 Trivette, A., Nargi, R.S., et al. (2020). Potently neutralizing and protective human antibodies against  
 353 SARS-CoV-2. *Nature* *584*, 443-449. 10.1038/s41586-020-2548-6.



- 354 16. Westendorf, K., Zentelis, S., Wang, L., Foster, D., Vaillancourt, P., Wiggin, M., Lovett, E., van der Lee,  
355 R., Hendle, J., Pustilnik, A., et al. (2022). LY-CoV1404 (bebtelovimab) potently neutralizes SARS-CoV-  
356 2 variants. *Cell Rep* 39, 110812. 10.1016/j.celrep.2022.110812.
- 357 17. Pinto, D., Park, Y.J., Beltramello, M., Walls, A.C., Tortorici, M.A., Bianchi, S., Jaconi, S., Culap, K.,  
358 Zatta, F., De Marco, A., et al. (2020). Cross-neutralization of SARS-CoV-2 by a human monoclonal  
359 SARS-CoV antibody. *Nature* 583, 290-295. 10.1038/s41586-020-2349-y.
- 360 18. Fenwick, C., Turelli, P., Ni, D., Perez, L., Lau, K., Herate, C., Marlin, R., Lana, E., Pellaton, C., Raclot,  
361 C., et al. (2022). Patient-derived monoclonal antibody neutralizes SARS-CoV-2 Omicron variants and  
362 confers full protection in monkeys. *Nat Microbiol* 7, 1376-1389. 10.1038/s41564-022-01198-6.
- 363 19. Luo, S., Zhang, J., Kreuzberger, A.J.B., Eaton, A., Edwards, R.J., Jing, C., Dai, H.Q., Sempowski, G.D.,  
364 Cronin, K., Parks, R., et al. (2022). An antibody from single human VH-rearranging mouse neutralizes  
365 all SARS-CoV-2 variants through BA.5 by inhibiting membrane fusion. *Sci Immunol* 7, eadd5446.  
366 10.1126/sciimmunol.add5446.
- 367 20. Cao, Y., Yisimayi, A., Jian, F., Song, W., Xiao, T., Wang, L., Du, S., Wang, J., Li, Q., Chen, X., et al.  
368 (2022). BA.2.12.1, BA.4 and BA.5 escape antibodies elicited by Omicron infection. *Nature* 608, 593-  
369 602. 10.1038/s41586-022-04980-y.
- 370 21. Du, S., Liu, P., Zhang, Z., Xiao, T., Yasimayi, A., Huang, W., Wang, Y., Cao, Y., Xie, X.S., and Xiao, J.  
371 (2021). Structures of SARS-CoV-2 B.1.351 neutralizing antibodies provide insights into cocktail  
372 design against concerning variants. *Cell Res* 31, 1130-1133. 10.1038/s41422-021-00555-0.
- 373 22. Wang, X., Chen, X., Tan, J., Yue, S., Zhou, R., Xu, Y., Lin, Y., Yang, Y., Zhou, Y., Deng, K., et al. (2022).  
374 35B5 antibody potently neutralizes SARS-CoV-2 Omicron by disrupting the N-glycan switch via a  
375 conserved spike epitope. *Cell Host Microbe* 30, 887-895 e884. 10.1016/j.chom.2022.03.035.
- 376 23. Liu, L., Iketani, S., Guo, Y., Casner, R.G., Reddem, E.R., Nair, M.S., Yu, J., Chan, J.F., Wang, M.,  
377 Cerutti, G., et al. (2022). An antibody class with a common CDRH3 motif broadly neutralizes  
378 sarbecoviruses. *Sci Transl Med*, eabn6859. 10.1126/scitranslmed.abn6859.
- 379 24. Wang, Z., Muecksch, F., Cho, A., Gaebler, C., Hoffmann, H.H., Ramos, V., Zong, S., Cipolla, M.,  
380 Johnson, B., Schmidt, F., et al. (2022). Analysis of memory B cells identifies conserved neutralizing  
381 epitopes on the N-terminal domain of variant SARS-Cov-2 spike proteins. *Immunity* 55, 998-1012  
382 e1018. 10.1016/j.immuni.2022.04.003.
- 383 25. Hong, Q., Han, W., Li, J., Xu, S., Wang, Y., Xu, C., Li, Z., Wang, Y., Zhang, C., Huang, Z., and Cong, Y.  
384 (2022). Molecular basis of receptor binding and antibody neutralization of Omicron. *Nature* 604,  
385 546-552. 10.1038/s41586-022-04581-9.
- 386 26. Starr, T.N., Greaney, A.J., Stewart, C.M., Walls, A.C., Hannon, W.W., Veessler, D., and Bloom, J.D.  
387 (2022). Deep mutational scans for ACE2 binding, RBD expression, and antibody escape in the SARS-  
388 CoV-2 Omicron BA.1 and BA.2 receptor-binding domains. *bioRxiv*, 2022.2009.2020.508745.  
389 10.1101/2022.09.20.508745.
- 390 27. Wang, Q., Bowen, A., Valdez, R., Gherasim, C., Gordon, A., Liu, L., and Ho, D.D. (2022). Antibody  
391 responses to Omicron BA.4/BA.5 bivalent mRNA vaccine booster shot. *bioRxiv*,  
392 2022.2010.2022.513349. 10.1101/2022.10.22.513349.
- 393 28. Tenforde, M.W., Self, W.H., Adams, K., Gaglani, M., Ginde, A.A., McNeal, T., Ghamande, S., Douin,  
394 D.J., Talbot, H.K., Casey, J.D., et al. (2021). Association Between mRNA Vaccination and COVID-19  
395 Hospitalization and Disease Severity. *JAMA* 326, 2043-2054. 10.1001/jama.2021.19499.
- 396 29. Lin, D.Y., Gu, Y., Xu, Y., Wheeler, B., Young, H., Sunny, S.K., Moore, Z., and Zeng, D. (2022).  
397 Association of Primary and Booster Vaccination and Prior Infection With SARS-CoV-2 Infection and  
398 Severe COVID-19 Outcomes. *JAMA* 328, 1415-1426. 10.1001/jama.2022.17876.
- 399 30. Havers, F.P., Pham, H., Taylor, C.A., Whitaker, M., Patel, K., Anglin, O., Kambhampati, A.K., Milucky,  
400 J., Zell, E., Moline, H.L., et al. (2022). COVID-19-Associated Hospitalizations Among Vaccinated and

- 401 Unvaccinated Adults 18 Years or Older in 13 US States, January 2021 to April 2022. *JAMA Intern*  
402 *Med* 182, 1071-1081. 10.1001/jamainternmed.2022.4299.
- 403 31. Price, A.M., Olson, S.M., Newhams, M.M., Halasa, N.B., Boom, J.A., Sahni, L.C., Pannaraj, P.S., Irby,  
404 K., Bline, K.E., Maddux, A.B., et al. (2022). BNT162b2 Protection against the Omicron Variant in  
405 Children and Adolescents. *N Engl J Med* 386, 1899-1909. 10.1056/NEJMoa2202826.
- 406 32. Azzolini, E., Levi, R., Sarti, R., Pozzi, C., Mollura, M., Mantovani, A., and Rescigno, M. (2022).  
407 Association Between BNT162b2 Vaccination and Long COVID After Infections Not Requiring  
408 Hospitalization in Health Care Workers. *JAMA* 328, 676-678. 10.1001/jama.2022.11691.
- 409 33. Al-Aly, Z., Bowe, B., and Xie, Y. (2022). Long COVID after breakthrough SARS-CoV-2 infection. *Nat*  
410 *Med* 28, 1461-1467. 10.1038/s41591-022-01840-0.
- 411 34. Ayoubkhani, D., Bosworth, M.L., King, S., Pouwels, K.B., Glickman, M., Nafilyan, V., Zaccardi, F.,  
412 Khunti, K., Alwan, N.A., and Walker, A.S. (2022). Risk of Long COVID in People Infected With Severe  
413 Acute Respiratory Syndrome Coronavirus 2 After 2 Doses of a Coronavirus Disease 2019 Vaccine:  
414 Community-Based, Matched Cohort Study. *Open Forum Infect Dis* 9, ofac464.  
415 10.1093/ofid/ofac464.
- 416 35. Wang, P., Nair, M.S., Liu, L., Iketani, S., Luo, Y., Guo, Y., Wang, M., Yu, J., Zhang, B., Kwong, P.D., et  
417 al. (2021). Antibody resistance of SARS-CoV-2 variants B.1.351 and B.1.1.7. *Nature* 593, 130-135.  
418 10.1038/s41586-021-03398-2.
- 419 36. O'Toole, A., Scher, E., Underwood, A., Jackson, B., Hill, V., McCrone, J.T., Colquhoun, R., Ruis, C.,  
420 Abu-Dahab, K., Taylor, B., et al. (2021). Assignment of epidemiological lineages in an emerging  
421 pandemic using the pangolin tool. *Virus Evol* 7, veab064. 10.1093/ve/veab064.
- 422 37. Chan, K.K., Dorosky, D., Sharma, P., Abbasi, S.A., Dye, J.M., Kranz, D.M., Herbert, A.S., and Procko, E.  
423 (2020). Engineering human ACE2 to optimize binding to the spike protein of SARS coronavirus 2.  
424 *Science* 369, 1261-1265. 10.1126/science.abc0870.
- 425 38. Martin, M. (2011). Cutadapt removes adapter sequences from high-throughput sequencing reads.  
426 2011 17, 3. 10.14806/ej.17.1.200.
- 427 39. Langmead, B., and Salzberg, S.L. (2012). Fast gapped-read alignment with Bowtie 2. *Nat Methods* 9,  
428 357-359. 10.1038/nmeth.1923.
- 429 40. Robinson, J.T., Thorvaldsdottir, H., Winckler, W., Guttman, M., Lander, E.S., Getz, G., and Mesirov,  
430 J.P. (2011). Integrative genomics viewer. *Nat Biotechnol* 29, 24-26. 10.1038/nbt.1754.
- 431 41. Simon, V., Kota, V., Bloomquist, R.F., Hanley, H.B., Forgacs, D., Pahwa, S., Pallikkuth, S., Miller, L.G.,  
432 Schaenman, J., Yeaman, M.R., et al. (2022). PARIS and SPARTA: Finding the Achilles' Heel of SARS-  
433 CoV-2. *mSphere* 7, e0017922. 10.1128/msphere.00179-22.
- 434 42. Liu, L., Wang, P., Nair, M.S., Yu, J., Rapp, M., Wang, Q., Luo, Y., Chan, J.F., Sahi, V., Figueroa, A., et al.  
435 (2020). Potent neutralizing antibodies against multiple epitopes on SARS-CoV-2 spike. *Nature* 584,  
436 450-456. 10.1038/s41586-020-2571-7.
- 437 43. Baym, M., Kryazhimskiy, S., Lieberman, T.D., Chung, H., Desai, M.M., and Kishony, R. (2015).  
438 Inexpensive multiplexed library preparation for megabase-sized genomes. *PLoS One* 10, e0128036.  
439 10.1371/journal.pone.0128036.
- 440 44. Wrapp, D., Wang, N., Corbett, K.S., Goldsmith, J.A., Hsieh, C.L., Abiona, O., Graham, B.S., and  
441 McLellan, J.S. (2020). Cryo-EM structure of the 2019-nCoV spike in the prefusion conformation.  
442 *Science* 367, 1260-1263. 10.1126/science.abb2507.
- 443 45. Wilks, S.H., Muhlemann, B., Shen, X., Tureli, S., LeGresley, E.B., Netzl, A., Caniza, M.A., Chacaltana-  
444 Huarcaya, J.N., Corman, V.M., Daniell, X., et al. (2022). Mapping SARS-CoV-2 antigenic relationships  
445 and serological responses. *bioRxiv*. 10.1101/2022.01.28.477987.

## 447 STAR METHODS

448

## 449 KEY RESOURCE TABLE

REAGENT or RESOURCE	SOURCE	IDENTIFIER
Antibodies		
C1520	Wang et al., 2022 <sup>24</sup>	N/A
C1717	Wang et al., 2022 <sup>24</sup>	N/A
S3H3	Hong et al., 2022 <sup>25</sup>	N/A
S2K146	Park et al., 2022 <sup>9</sup>	N/A
Omi-3	Nutalai et al., 2022 <sup>10</sup>	N/A
Omi-18	Nutalai et al., 2022 <sup>10</sup>	N/A
BD-515	Cao et al., 2021 <sup>11</sup>	N/A
XGv051	Wang et al., 2022 <sup>12</sup>	N/A
XGv347	Wang et al., 2022 <sup>13</sup>	N/A
ZCB11	Zhou et al., 2022 <sup>14</sup>	N/A
COV2-2196	Zost et al., 2020 <sup>15</sup>	N/A
LY-CoV1404	Westendorf et al., 2022 <sup>16</sup>	N/A
XGv289	Wang et al., 2022 <sup>13</sup>	N/A
XGv264	Wang et al., 2022 <sup>12</sup>	N/A
S309	Pinto et al., 2020 <sup>17</sup>	N/A
P2G3	Fenwick et al., 2022 <sup>18</sup>	N/A
SP1-77	Luo et al., 2022 <sup>19</sup>	N/A
BD55-5840	Cao et al., 2022 <sup>20</sup>	N/A
XGv282	Wang et al., 2022 <sup>13</sup>	N/A
BD-804	Du et al., 2021 <sup>21</sup>	N/A
35B5	Wang et al., 2022 <sup>22</sup>	N/A
COV2-2130	Zost et al., 2020 <sup>15</sup>	N/A
10-40	Liu et al., 2022 <sup>23</sup>	N/A
Bacterial and virus strains		
VSV-G pseudotyped $\Delta$ G-luciferase	Kerafast	Cat#EH1020-PM
Biological samples		
Sera from 3 shots of mRNA-vaccinated individuals (3 shots WT)	Wang et al., 2022 <sup>27</sup>	N/A
Sera from 4 shots of mRNA-vaccinated individuals (4 shots WT)	Wang et al., 2022 <sup>27</sup>	N/A
Bivalent vaccine booster sera (3 shots WT+ bivalent)	Wang et al., 2022 <sup>27</sup>	N/A
BA.2 breakthrough sera	This paper	N/A
BA.5 breakthrough sera	Wang et al., 2022 <sup>27</sup>	N/A
Chemicals, peptides, and recombinant proteins		
Polyethylenimine (PEI)	Polysciences Inc.	Cat#23966-100
hACE2	This paper	N/A
SARS-CoV-2 BA.4/5 S2P	Wang et al., 2022 <sup>2</sup>	N/A
SARS-CoV-2 BQ.1 S2P	This paper	N/A
SARS-CoV-2 BQ.1.1 S2P	This paper	N/A
SARS-CoV-2 BA.2 S2P	Wang et al., 2022 <sup>2</sup>	N/A

SARS-CoV-2 XBB S2P	This paper	N/A
SARS-CoV-2 XBB.1 S2P	This paper	N/A
Critical commercial assays		
Luciferase Assay System	Promega	Cat#E4550
Series S sensor chip CM5	Cytiva	Cat#BR100530
His-capture kit	Cytiva	Cat#28995056
Experimental models: cell lines		
HEK293T	ATCC	Cat#CRL-3216; RRID: CVCL_0063
Vero-E6	ATCC	Cat#CRL-1586; RRID: CVCL_0574
Expi293 cells	Thermo Fisher Scientific	Cat#A14527; RRID: CVCL_D615
Recombinant DNA		
pCMV3-D614G	Wang et al., 2022 <sup>2</sup>	N/A
pCMV3-BA.4/5	Wang et al., 2022 <sup>2</sup>	N/A
pCMV3-BQ.1	This paper	N/A
pCMV3-BQ.1.1	This paper	N/A
pCMV3-BA.4/5-R346T	Wang et al., 2022 <sup>5</sup>	N/A
pCMV3-BA.4/5-K444T	This paper	N/A
pCMV3-BA.4/5-N460K	This paper	N/A
pCMV3-BA.2	Wang et al., 2022 <sup>2</sup>	N/A
pCMV3-XBB	This paper	N/A
pCMV3-XBB.1	This paper	N/A
pCMV3-BA.2-V83A	This paper	N/A
pCMV3-BA.2-Del144	This paper	N/A
pCMV3-BA.2-H146Q	This paper	N/A
pCMV3-BA.2-Q183E	This paper	N/A
pCMV3-BA.2-V213E	This paper	N/A
pCMV3-BA.2-G252V	This paper	N/A
pCMV3-BA.2-G339H	Wang et al., 2022 <sup>2</sup>	N/A
pCMV3-BA.2-R346T	This paper	N/A
pCMV3-BA.2-L368I	This paper	N/A
pCMV3-BA.2-V445P	This paper	N/A
pCMV3-BA.2-G446S	Wang et al., 2022 <sup>2</sup>	N/A
pCMV3-BA.2-N460K	Wang et al., 2022 <sup>2</sup>	N/A
pCMV3-BA.2-F486S	This paper	N/A
pCMV3-BA.2-F490S	This paper	N/A
pCMV3-BA.2-R493Q	Wang et al., 2022 <sup>2</sup>	N/A
paH-BA.4/5 S2P	Wang et al., 2022 <sup>2</sup>	N/A
paH-BQ.1 S2P	This paper	N/A
paH-BQ.1.1 S2P	This paper	N/A
paH-BA.2 S2P	Wang et al., 2022 <sup>2</sup>	N/A
paH-XBB S2P	This paper	N/A
paH-XBB.1 S2P	This paper	N/A
pcDNA3-sACE2-WT (732)-IgG1	Chan et al., 2020 <sup>37</sup>	RRID: Addgene_154104
Software and algorithms		
Cutadapt v2.1	Martin, 2011 <sup>38</sup>	<a href="https://cutadapt.readthedocs.io/en/v2.1/">https://cutadapt.readthedocs.io/en/v2.1/</a>

Bowtie2 v2.3.4	Langmead et al.,2012 <sup>39</sup>	<a href="https://github.com/BenLangmead/bowtie2">https://github.com/BenLangmead/bowtie2</a>
Integrative Genomics Viewer	Robinson et al., 2011 <sup>40</sup>	<a href="https://software.broadinstitute.org/software/igv/">https://software.broadinstitute.org/software/igv/</a>
GraphPad Prism 9	Dotmatics	<a href="https://www.graphpad.com/scientific-software/prism/">https://www.graphpad.com/scientific-software/prism/</a>
PyMOL v.2.3.2	Schrödinger, LLC	<a href="https://pymol.org/2/#page-top">https://pymol.org/2/#page-top</a>
Biacore T200 Evaluation Software (Version 1.0)	Cytiva	N/A
Racmacs version 1.1.35	Smith et al., 2004 <sup>7</sup>	<a href="https://acorg.github.io/Racmacs/">https://acorg.github.io/Racmacs/</a>

450

451 **RESOURCE AVAILABILITY**452 **Lead contact**

453 Further information and requests for resources should be directed to and will be fulfilled by the  
454 lead contact, David D. Ho (dh2994@cumc.columbia.edu).

455 **Materials availability**

456 All requests for resources and reagents should be directed to and will be fulfilled by the Lead  
457 Contact, David D. Ho (dh2994@cumc.columbia.edu). This includes selective cell lines, plasmids,  
458 antibodies, viruses, serum, and proteins. All reagents will be made available on request after  
459 completion of a Material Transfer Agreement.

460 **Data and code availability**461 **• Data**

462 Data reported in this paper will be shared by the lead contact upon request.

463 **• Code**

464 This paper does not report original code.

465 **• All other items**

466 Any additional information required to reanalyze the data reported in this paper is available from  
467 the lead contact upon request.

468

469 **EXPERIMENTAL MODEL AND SUBJECTS**470 **Human subjects**

471 Sera analyzed in this study were categorized into several cohorts. “3 shots WT” samples were sera  
472 from individuals who had received three doses of monovalent, referred to as wild-type (WT)  
473 mRNA vaccines (either Moderna mRNA-1273 or Pfizer BNT162b2). Sera were also collected

474 from individuals after a fourth monovalent mRNA vaccine (referred to as “4 shots WT”). Bivalent  
475 vaccine sera were collected from individuals who had received three monovalent mRNA vaccine  
476 doses followed by one dose of the Pfizer or Moderna bivalent vaccine targeting BA.4/BA.5 in  
477 addition to the ancestral D614G variant. “BA.2 breakthrough” and “BA.4/BA.5 breakthrough”  
478 sera were collected from individuals who had received monovalent mRNA vaccines followed by  
479 infection with Omicron subvariants BA.2 and BA.4 or BA.5, respectively. Samples were examined  
480 by anti-nucleoprotein (NP) ELISA to confirm status of prior SARS-CoV-2 infection. Clinical  
481 information for the different study cohorts is summarized in **Table S1**.

482 A subset of sera analyzed in this study was collected at Columbia University Irving  
483 Medical Center. Subjects provided written informed consent, and serum collections were  
484 performed under protocols reviewed and approved by the Institutional Review Board of Columbia  
485 University.

486 Additional serum samples included in this study were collected at the University of  
487 Michigan through the Immunity-Associated with SARS-CoV-2 Study (IASO), which is an  
488 ongoing cohort study in Ann Arbor, Michigan that began in 2020<sup>41</sup>. IASO participants provided  
489 written informed consent and all serum samples were collected under the protocol reviewed and  
490 approved by the Institutional Review Board of the University of Michigan Medical School.

491

## 492 **Cell lines**

493 Vero-E6 cells (CRL-1586) and HEK293T cells (CRL-3216) were purchased from the ATCC.  
494 Expi293 cells (A14527) were purchased from Thermo Fisher Scientific. Morphology of each cell  
495 line was confirmed visually before use. All cell lines tested mycoplasma negative. Vero-E6 cells  
496 are from African green monkey kidneys. HEK293T cells and Expi293 cells are of female origin.

497

## 498 **METHOD DETAILS**

### 499 **Monoclonal antibodies**

500 Antibodies were generated as previously described<sup>42</sup>. The variable regions of heavy and light  
501 chains for each antibody were synthesized (GenScript), cloned into gWiz or pCDNA3.4 vector,  
502 then transfected into Expi293 cells (Thermo Fisher Scientific) using 1 mg/mL polyethylenimine  
503 (PEI), and purified from the supernatant by affinity purification using rProtein A Sepharose (GE).

504

### 505 **Variant SARS-CoV-2 spike plasmid construction**

506 Spike-expressing plasmids for D614G, BA.2, and BA.4/5 were previously generated<sup>2</sup>. Plasmids  
507 expressing the spike genes of BQ.1, BQ.1.1, XBB, and XBB.1, as well as the individual mutations  
508 found in the four variants in the background of BA.4/5 or BA.2 were generated by an in-house  
509 high-throughput template-guide gene synthesis approach, as previously described<sup>1</sup>. Briefly, 5'-  
510 phosphorylated oligo pools with designed mutations were annealed to the template of the BA.2 or  
511 BA.4/5 spike gene construct and extended by high fidelity DNA polymerase. Taq DNA ligase was  
512 used to seal nicks between extension products, which were subsequently amplified by PCR to  
513 generate variants of interest. Next generation sequencing<sup>43</sup> was performed on the Illumina Miseq  
514 platform (single-end mode with 50 bp R1) to verify the sequences of variants. Cutadapt v2.1<sup>38</sup> and  
515 Bowtie2 v2.3.4<sup>39</sup> were used to analyze raw reads to get the resulting read alignments, which were  
516 then visualized in Integrative Genomics Viewer<sup>40</sup>.

517 To make the expression constructs for soluble spike trimer proteins, we subcloned the  
518 ectodomain (1-1208aa in WA1) of the spike into the paH vector and then introduced K986P and  
519 V987P substitutions as well as a “GSAS” substitution of the furin cleavage site (682-685aa in  
520 WA1) into the spike<sup>44</sup>. All constructs were confirmed by Sanger sequencing.

521

### 522 **Protein expression and purification**

523 To make human ACE2 protein, pcDNA3-sACE2-WT(732)-IgG1<sup>37</sup> (Addgene plasmid #154104,  
524 gift of Erik Procko) plasmid was transfected into Expi293 cells using PEI at a ratio of 1:3, and the  
525 supernatants were collected after five days. hACE2 was purified from the cell supernatant by using  
526 rProtein A Sepharose (GE) followed by running through a Superdex 200 Increase 10/300 GL  
527 column. For the spike trimer proteins, paH-spike was transfected into Expi293 cells using PEI at  
528 a ratio of 1:3, and the supernatants were collected five days later. The spike proteins were purified  
529 using Excel resin (Cytiva) according to the manufacturer's instructions. The molecular weight and  
530 purity were checked by running the proteins on SDS-PAGE.

531

### 532 **Surface plasmon resonance (SPR)**

533 The CM5 chip was immobilized with anti-His antibodies using the His Capture Kit (Cytiva) to  
534 capture the spike protein through their C-terminal His-tag. Serially diluted human ACE2-Fc  
535 protein was then flowed over the chip in HBS-EP+ buffer (Cytiva). Binding affinities were

536 measured with the Biacore T200 system at 25°C in the single-cycle mode. Data was analyzed by  
537 the Evaluation Software using the 1:1 binding model.

538

### 539 **Pseudovirus production**

540 SARS-CoV-2 pseudoviruses were generated as previously described<sup>42</sup>. In brief, HEK293T cells  
541 were transfected with a spike-expressing construct using 1 mg/mL PEI and then infected with  
542 VSV-G pseudotyped  $\Delta$ G-luciferase (G\* $\Delta$ G-luciferase, Kerafast) one day post-transfection. 2  
543 hours after infection, cells were washed three times with PBS, changed to fresh medium, and then  
544 cultured for one more day before the cell supernatants were harvested. Pseudoviruses in the cell  
545 supernatants were clarified by centrifugation, aliquoted, and stored at -80°C.

546

### 547 **Pseudovirus neutralization assay**

548 Pseudoviruses were titrated on Vero-E6 cells before conducting the neutralization assays to  
549 normalize the viral input between assays. Heat-inactivated sera were serially diluted starting from  
550 1:100 with a dilution factor of four and antibodies were 5-fold serially diluted starting from 10  
551  $\mu$ g/mL in 96 well plates in triplicate. Then, 50  $\mu$ L of diluted pseudovirus was added and incubated  
552 with 50  $\mu$ L serial dilutions of serum or antibody for 1 hour at 37°C. During the co-culture, Vero-  
553 E6 cells were trypsinized, resuspended with fresh medium, and then added into virus-sample  
554 mixture at a density of  $4 \times 10^4$  cells/well. The plates were incubated at 37°C for ~12 hours before  
555 luciferase activity was quantified using the Luciferase Assay System (Promega) using SoftMax  
556 Pro v.7.0.2 (Molecular Devices). Neutralization ID<sub>50</sub> values for sera and IC<sub>50</sub> values for antibodies  
557 were calculated by fitting a nonlinear five-parameter dose-response curve to the data in GraphPad  
558 Prism v.9.2.

559

### 560 **Antibody footprint and mutagenesis analysis**

561 All the structures were downloaded from the Protein Data Bank (7XIV (BA.2 spike), 7WK9  
562 (S3H3), 7UAR (C1717), 7UAP (C1520), 7TAS (S2K146), 7XCO (S309), 7WRZ (BD55-5840),  
563 7ZF3 (Omi-3), 7ZFB (Omi-18), 7E88 (BD-515), 7WED (XGv347), 7XH8 (ZCB11), 7SD5 (10-  
564 40), 7WM0 (35B5), 7WLC (XGv282), 7WE9 (XGv289), 7UPY (SP1-77), 7QTK (P2G3), 7MMO  
565 (LY-CoV1404), 7EYA (BD-804)) for analysis. The interface residues were obtained by running  
566 the InterfaceResidues script from PyMOLWiki in PyMOL, and the edge of these residues was



567 defined as the footprint of the antibodies. Site-directed mutagenesis was also conducted in PyMOL.  
568 All the structural analysis figures were generated in PyMOL v.2.3.2 (Schrödinger, LLC).

569

### 570 **Antigenic cartography**

571 We constructed an antigenic map based on the serum neutralization data by utilizing the antigenic  
572 cartography technique as previously described<sup>45</sup>. The antigenic map was generated using the  
573 Racmacs package (<https://acorg.github.io/Racmacs/>, version 1.1.35) in R with 1000 optimization  
574 steps, a dilution step size of zero, and the minimum column basis parameter set to “none”. All  
575 distances between virus and serum positions on the antigenic map were optimized such that  
576 distances correspond to the fold decrease in neutralizing ID<sub>50</sub> titer, relative to the maximum titer  
577 for each serum. Each unit of distance in any direction in the antigenic map corresponds to a two-  
578 fold change in the ID<sub>50</sub> titer.

579

### 580 **QUANTIFICATION AND STATISTICAL ANALYSIS**

581 IC<sub>50</sub> and ID<sub>50</sub> values were determined by fitting the data to five-parameter dose-response curves  
582 in GraphPad Prism v.9.2. Comparisons were made by two-tailed Wilcoxon matched-pairs signed-  
583 rank tests. \*\*\* $p < 0.001$ ; \*\*\*\* $p < 0.0001$ .

Figure 1

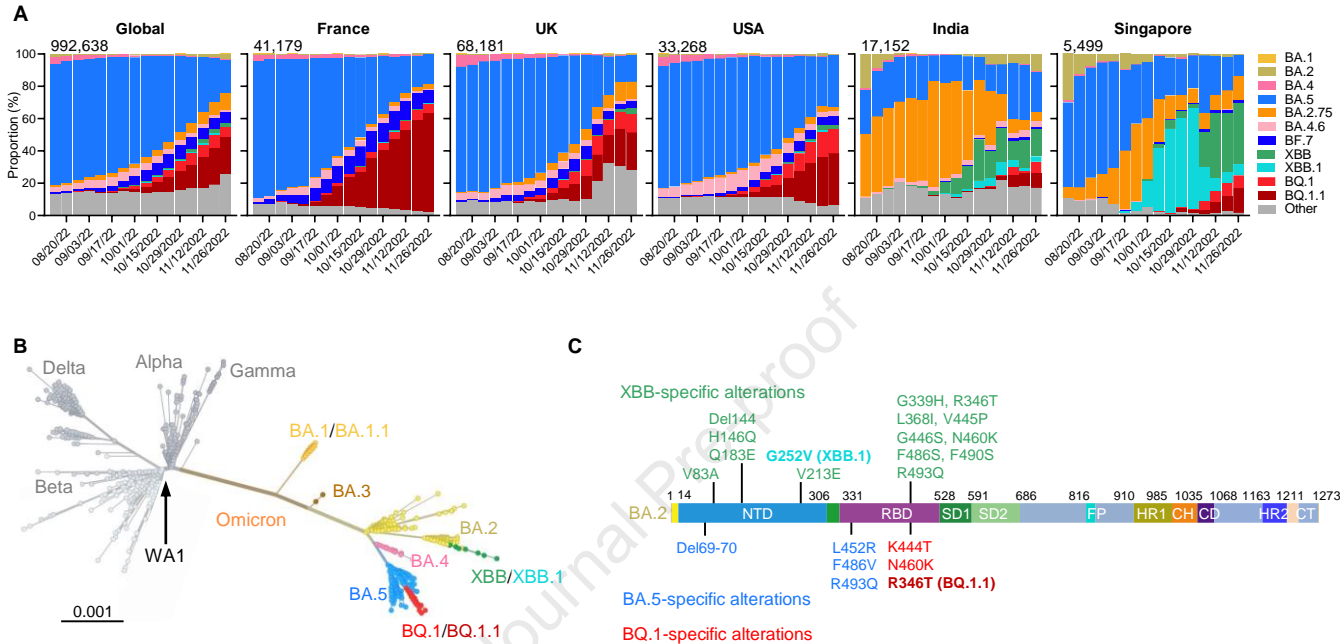


**Figure 2**

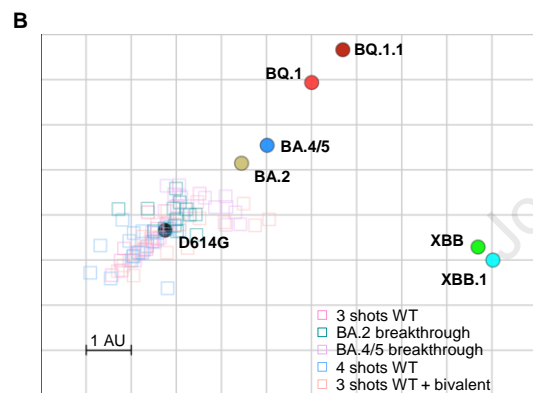
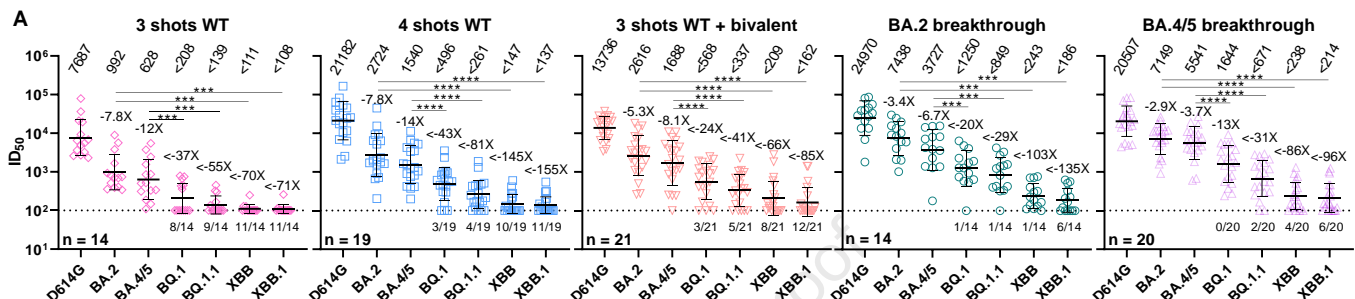
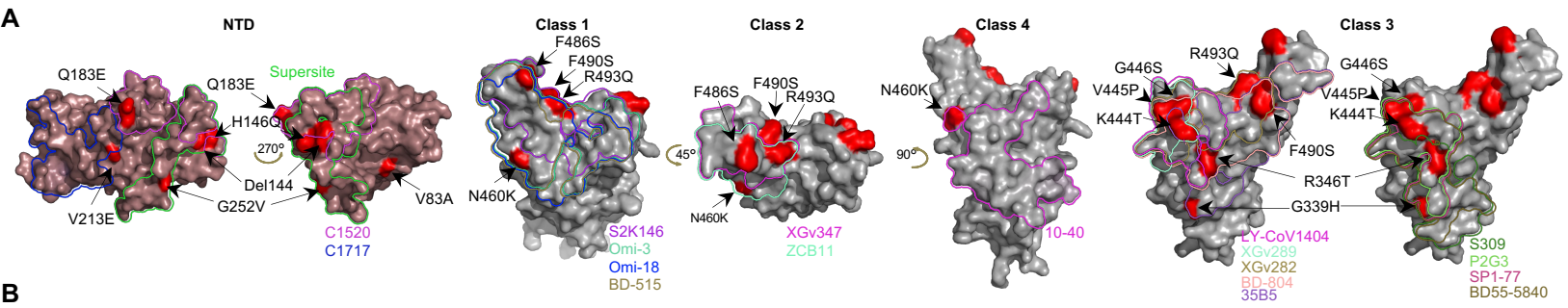


Figure 3



Fold change in IC <sub>50</sub>	NTD	NTD-SD2	SD1	RBD Class 1				RBD Class 2				RBD Class 3								RBD Class 4	Evusheld					
	C1520	C1717	S3H3	S2K146	Omi-3	Omi-18	BD-515	XGv051	XGv347	ZCB11	COV2-2196	LY-CoV1404	XGv289	XGv264	S309	P2G3	SP1-77	BD55-5840	XGv282	BD-804		35B5	COV2-2130	10-40		
Relative to BA.4/5	BQ.1	1.4	-3.2	-1.4	-6.5	-38	-10	-34	-3.2	1.2	<-2.1	NA	<-7668	-11	-206	-1.2	-729	-3538	-3.9	-22	<-520	NA	<-472	-4.1	<-284	
	BQ.1.1	-2.3	-5.3	-1.8	-5.9	-36	-14	-37	-3.8	-1.0	<-2.1	NA	<-7668	-27	<-4173	-4.2	<-4532	<-1922	<-1125	-105	<-520	NA	<-472	-4.1	<-284	
	BA.4/5-R346T	-1.2	1.5	-1.5	1.1	1.2	1.3	1.6	1.2	1.6	1.9	NA	1.2	-1.2	-1.3	-3.4	-19	<-1922	-163	-1.1	<-520	NA	<-472	-2.1	<-284	
	BA.4/5-K444T	-1.1	1.8	1.5	-1.2	1.4	1.2	1.6	1.2	-1.4	1.3	NA	<-7668	-4.3	-114	-1.1	-564	-770	-4.3	-6.3	<-520	NA	<-472	-2.9	<-284	
	BA.4/5-N460K	-1.6	-5.6	-1.2	-6.0	-57	-15	-43	-3.1	1.1	<-2.1	NA	-1.3	-9.3	-1.1	-1.8	-1.2	-1.7	-1.3	-1.9	-6.4	NA	-1.4	-4.1	-1.8	
Relative to BA.2	XBB	<-6340	-1.5	-1.0	-8.0	-78	-92	-45	<-7195	<-3250	<-847	<-5.2	<-6861	<-150	<-3190	2.4	<-4687	<-1626	<-739	<-8886	<-266	<-12	<-1123	-1.1	<-530	
	XBB.1	<-6340	-1.2	-1.2	-6.8	-112	-119	-65	<-7195	<-3250	<-847	<-5.2	<-6861	<-150	<-3190	2.1	<-4687	<-1626	<-739	<-8886	<-266	<-12	<-1123	-1.1	<-530	
		BA.2-V83A	1.5	1.6	1.1	-1.3	-1.3	-1.4	-1.2	-1.7	-1.0	-1.1	-1.6	1.1	-1.0	1.4	1.3	-1.1	-1.1	-1.4	-1.2	-1.2	-1.5	-1.2	-1.1	-1.3
		BA.2-Del144	-1.1	1.1	1.4	1.1	-1.0	1.2	1.1	-1.1	1.3	1.5	-2.1	1.4	1.1	1.5	1.8	1.1	1.2	-1.0	1.3	1.2	2.4	-1.1	1.0	-1.1
		BA.2-H146Q	2.0	1.6	1.5	-1.2	1.3	1.2	1.3	-1.6	1.5	1.2	-1.5	-1.1	1.2	1.3	1.3	-1.2	-1.1	-1.4	1.6	-1.2	-1.3	-1.0	1.0	-1.0
		BA.2-Q183E	-204	1.8	-1.2	-1.2	-1.2	-1.3	-1.1	-1.4	-1.0	-1.1	-1.6	-1.0	-1.0	1.2	1.3	-1.1	-1.3	-1.5	-1.4	1.3	-1.2	-1.3	-1.1	-1.2
		BA.2-V213E	-1.1	1.4	1.2	-1.1	1.1	1.4	1.2	-1.2	1.2	2.1	-1.1	1.2	1.4	1.2	1.2	1.3	-1.0	-1.0	1.4	1.4	-1.5	-1.0	1.1	-1.0
		BA.2-G252V	1.3	-1.0	1.2	-1.1	1.2	1.2	1.4	-1.1	1.2	1.5	-1.2	1.1	1.4	1.3	1.5	-1.1	1.2	1.2	1.3	1.2	-1.1	-1.2	<-1.1	-1.4
		BA.2-G339H	1.4	1.2	-1.1	-1.2	-1.3	-1.1	-1.0	-1.6	1.4	1.2	-2.0	-1.1	-1.7	1.4	2.8	1.1	-1.2	-3.0	-1.7	-1.3	1.3	-1.3	1.0	-1.2
		BA.2-R346T	-1.7	1.5	1.3	1.6	1.6	1.7	1.8	1.1	1.7	1.7	-1.1	-1.2	1.4	-1.2	-1.7	-3.1	<-1626	-107	-1.1	-3.0	<-12	<-1123	1.1	-79
		BA.2-L368I	-1.9	1.2	-1.2	-1.0	1.5	1.2	1.3	-1.2	2.3	1.8	-1.4	1.1	2.2	1.3	1.4	1.2	1.1	-1.6	1.6	1.4	2.6	1.1	2.7	-1.0
		BA.2-V445P	1.4	1.3	-1.2	1.1	1.7	1.4	1.3	-1.4	1.5	1.5	-1.2	<-6861	<-150	-364	1.9	<-4687	-1.2	-1.1	<-8886	-42	1.7	<-1123	1.4	-166
		BA.2-G446S	-1.0	1.5	1.3	1.3	1.7	1.4	1.4	-1.0	-1.0	1.5	-1.4	-1.4	2.6	-1.2	1.2	-1.0	1.7	-1.1	-19	1.5	-1.2	-1.9	1.5	-1.5
		BA.2-N460K	-1.0	-2.4	1.3	-4.7	-51	-2.6	-29	-4.9	-1.2	-6.2	1.1	1.1	-5.3	-1.0	-1.1	-1.1	-1.8	-1.2	-1.5	-2.4	-1.5	<-1.1	-1.3	
	BA.2-F486S	-1.3	-1.2	1.9	<-358	-38	-2.1	-1.4	<-7195	<-3250	<-847	<-5.2	1.5	1.4	1.2	1.4	1.2	1.1	1.5	-1.3	-1.6	-2.7	-1.2	<-1.1	-1.2	
	BA.2-F490S	1.3	1.3	1.1	1.3	-2.2	1.4	1.6	1.2	-1.3	-1.0	1.7	1.2	2.3	1.5	1.5	1.3	1.1	1.3	<-8886	-1.3	<-12	-1.5	1.6	1.2	
	BA.2-R493Q	-2.1	1.7	-1.5	5.4	2.5	-1.1	1.9	2.3	2.6	7.0	56	-1.0	1.5	1.7	-1.3	1.2	-1.1	-1.6	9.8	>10	>3	<-3	<-10	<-100	

Figure 4

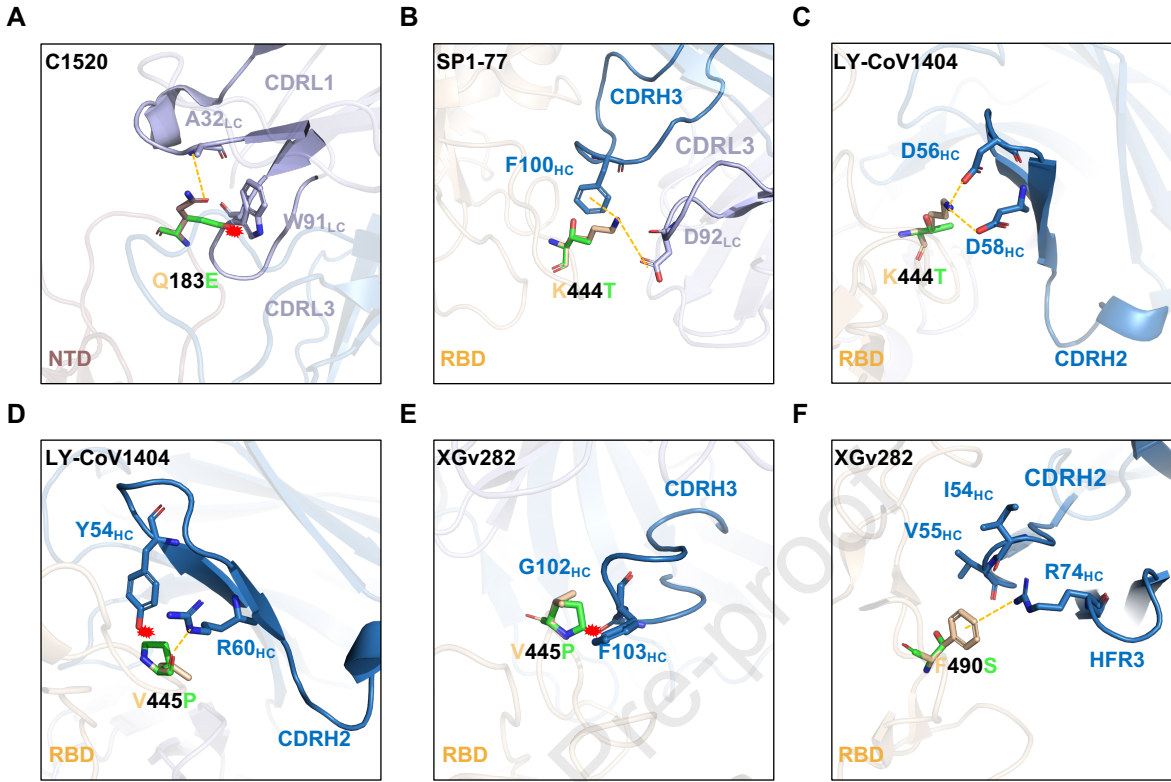


Figure 3

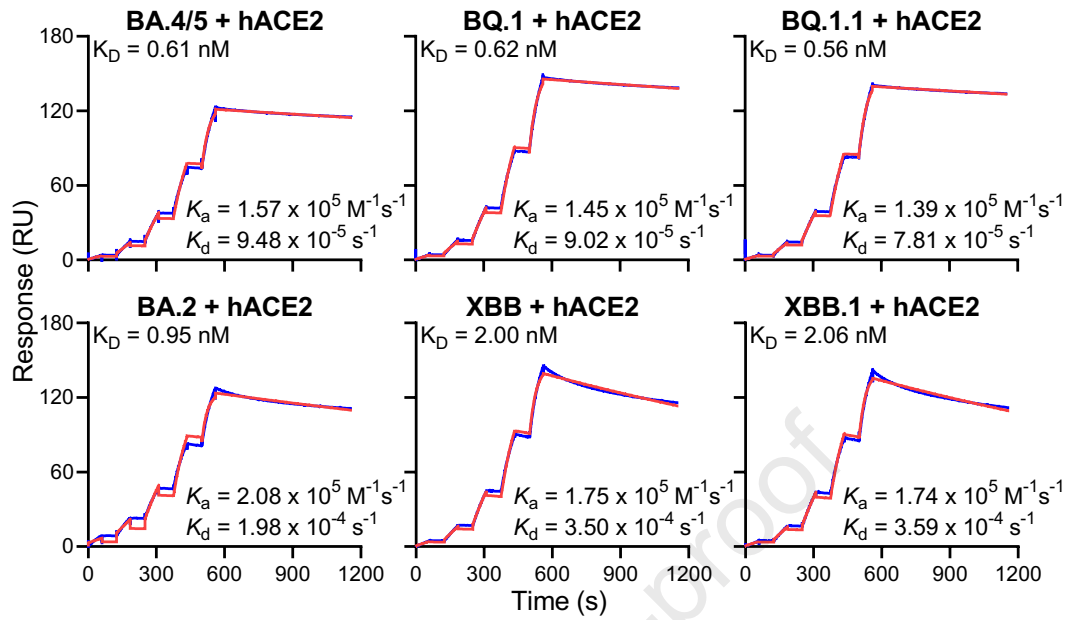


Figure S1

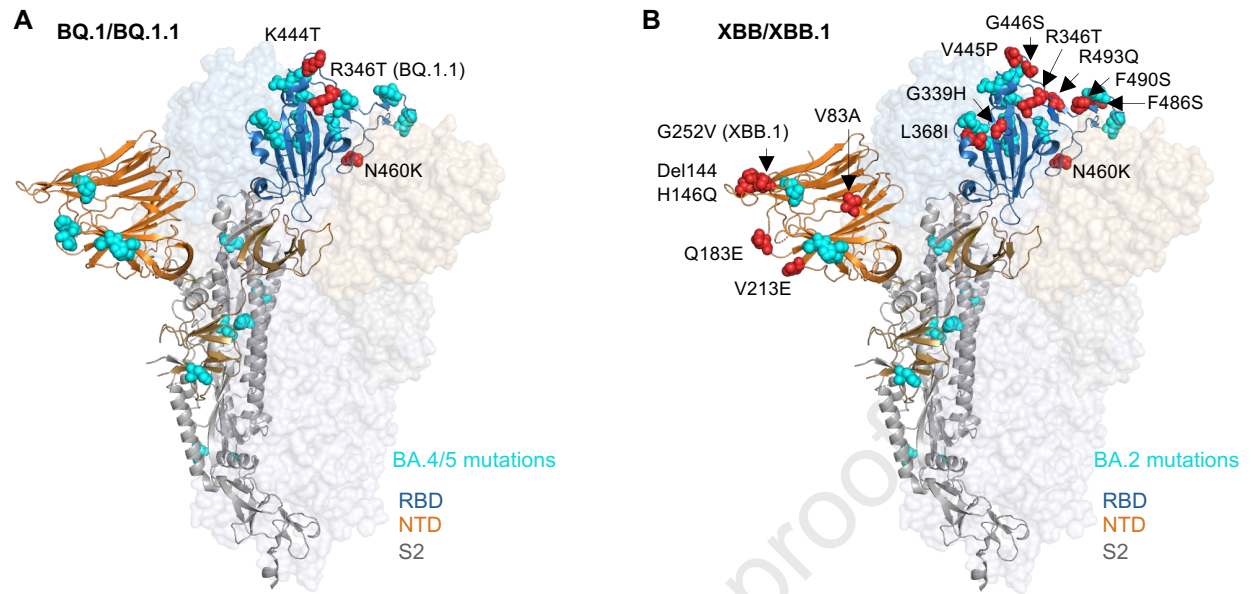
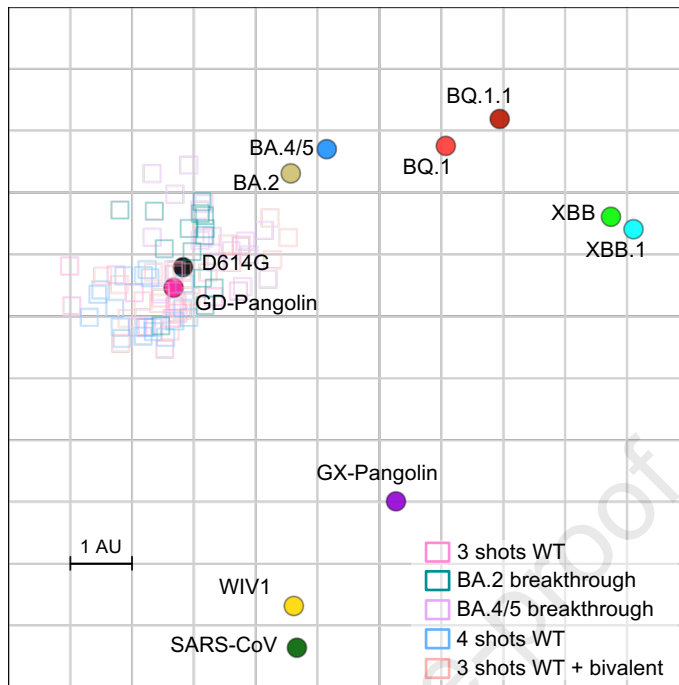


Figure S2

IC <sub>50</sub> (µg/ml)	NTD	NTD-SD2	SD1	RBD Class 1				RBD Class 2				RBD Class 3								RBD Class 4	Evusheld			
	C1520	C1717	S3H3	S2K146	Omi-3	Omi-18	BD-515	XGv051	XGv347	ZCB11	COV2-2196	LY-CoV1404	XGv289	XGv264	S309	P2G3	SP1-77	BD55-5840	XGv282	BD-804		35B5	COV2-2130	10-40
D614G	0.002	0.125	0.022	0.004	0.004	0.012	0.010	0.001	0.002	0.002	0.002	0.002	0.002	0.001	0.023	0.001	0.003	0.002	0.001	0.011	0.014	0.007	0.049	0.003
BA.4/5	0.001	0.209	0.014	0.090	0.023	0.013	0.010	0.050	3.450	4.868	>10	0.001	0.038	0.002	0.514	0.002	0.005	0.009	0.001	0.019	>10	0.021	2.414	0.035
BQ.1	0.001	0.666	0.019	0.585	0.860	0.131	0.343	0.159	2.830	>10	>10	>10	0.425	0.494	0.600	1.608	>10	0.034	0.020	>10	>10	>10	>10	>10
BQ.1.1	0.003	1.117	0.025	0.527	0.804	0.170	0.377	0.191	3.311	>10	>10	>10	1.013	>10	2.140	>10	>10	0.098	>10	>10	>10	>10	>10	>10
BA.4/5-R346T	0.002	0.141	0.020	0.081	0.019	0.009	0.006	0.042	2.166	2.560	>10	0.001	0.045	0.003	1.726	0.041	>10	1.447	0.001	>10	>10	>10	5.069	>10
BA.4/5-K444T	0.002	0.116	0.009	0.104	0.016	0.010	0.006	0.040	4.766	3.731	>10	>10	0.161	0.273	0.552	1.245	4.007	0.038	0.006	>10	>10	>10	6.976	>10
BA.4/5-N460K	0.002	1.166	0.016	0.542	1.279	0.186	0.431	0.152	3.046	>10	>10	0.002	0.353	0.003	0.934	0.003	0.009	0.012	0.002	0.122	>10	0.030	>10	0.063
BA.2	0.002	0.561	0.016	0.028	0.015	0.005	0.012	0.001	0.003	0.012	1.924	0.001	0.067	0.003	0.833	0.002	0.006	0.014	0.001	0.038	0.827	0.009	8.770	0.019
XBB	>10	0.836	0.016	0.223	1.181	0.468	0.555	>10	>10	>10	>10	>10	>10	>10	0.343	>10	>10	>10	>10	>10	>10	>10	>10	>10
XBB.1	>10	0.693	0.019	0.190	1.705	0.605	0.803	>10	>10	>10	>10	>10	>10	>10	0.405	>10	>10	>10	>10	>10	>10	>10	>10	>10
BA.2-V83A	0.001	0.354	0.015	0.036	0.019	0.007	0.015	0.002	0.003	0.013	3.039	0.001	0.070	0.002	0.641	0.002	0.007	0.019	0.001	0.045	1.274	0.011	>10	0.025
BA.2-Del144	0.002	0.501	0.011	0.026	0.016	0.004	0.011	0.002	0.002	0.008	4.134	0.001	0.063	0.002	0.455	0.002	0.005	0.014	0.001	0.031	0.341	0.010	8.766	0.021
BA.2-H146Q	0.001	0.356	0.011	0.032	0.011	0.004	0.009	0.002	0.002	0.010	2.924	0.002	0.055	0.002	0.641	0.003	0.007	0.019	0.001	0.044	1.107	0.009	9.106	0.019
BA.2-Q183E	0.322	0.307	0.019	0.034	0.018	0.006	0.014	0.002	0.003	0.013	3.098	0.001	0.067	0.003	0.649	0.002	0.008	0.020	0.002	0.028	1.019	0.011	9.251	0.022
BA.2-V213E	0.002	0.406	0.013	0.030	0.014	0.004	0.010	0.002	0.002	0.006	2.177	0.001	0.047	0.003	0.720	0.002	0.006	0.014	0.001	0.026	1.247	0.009	8.198	0.018
BA.2-G252V	0.001	0.577	0.013	0.030	0.012	0.004	0.008	0.002	0.003	0.008	2.258	0.001	0.048	0.002	0.564	0.002	0.005	0.012	0.001	0.032	0.939	0.011	>10	0.026
BA.2-G339H	0.001	0.485	0.017	0.034	0.020	0.006	0.012	0.002	0.002	0.010	3.876	0.002	0.114	0.002	0.302	0.002	0.007	0.040	0.002	0.050	0.661	0.012	8.575	0.023
BA.2-R346T	0.003	0.372	0.012	0.017	0.010	0.003	0.007	0.001	0.002	0.007	2.109	0.002	0.048	0.004	1.433	0.007	>10	1.442	0.001	0.112	>10	>10	7.767	1.486
BA.2-L368I	0.003	0.453	0.019	0.027	0.010	0.004	0.010	0.002	0.001	0.006	2.603	0.001	0.030	0.002	0.605	0.002	0.005	0.021	0.001	0.026	0.324	0.008	3.202	0.018
BA.2-V445P	0.001	0.433	0.019	0.026	0.009	0.004	0.009	0.002	0.002	0.008	2.313	>10	>10	1.141	0.428	>10	0.007	0.144	>10	1.582	0.486	>10	6.311	3.135
BA.2-G446S	0.002	0.367	0.012	0.021	0.009	0.004	0.009	0.001	0.003	0.008	2.614	0.002	0.026	0.004	0.686	0.002	0.004	0.014	0.022	0.026	0.965	0.017	5.774	0.029
BA.2-N460K	0.002	1.323	0.012	0.132	0.784	0.013	0.358	0.007	0.004	0.073	1.756	0.001	0.355	0.003	0.878	0.002	0.011	0.017	0.001	0.058	1.957	0.013	>10	0.025
BA.2-F486S	0.002	0.677	0.008	>10	0.583	0.011	0.017	>10	>10	>10	>10	0.001	0.049	0.003	0.581	0.002	0.006	0.009	0.002	0.060	2.264	0.011	>10	0.023
BA.2-F490S	0.001	0.428	0.014	0.022	0.033	0.004	0.008	0.001	0.004	0.012	1.105	0.001	0.030	0.002	0.564	0.002	0.006	0.011	>10	0.048	>10	0.013	5.337	0.016
BA.2-R493Q	0.003	0.338	0.024	0.005	0.006	0.006	0.006	0.001	0.001	0.002	0.034	0.001	0.045	0.002	1.109	0.002	0.007	0.022	0.000	0.010	1.175	0.010	3.419	0.008

>10	1-10	0.1-1	0.01-0.1	<0.01
-----	------	-------	----------	-------





**In Brief:**

Recent BQ and XBB subvariants of SARS-CoV-2 demonstrate dramatically increased ability to evade neutralizing antibodies, even those from people who received the bivalent mRNA booster or who are immunized and had previous breakthrough Omicron infection. Additionally, both BQ and XBB are completely resistant to bebtelovimab, meaning there are now no clinically authorized therapeutic antibodies effective against these circulating variants.

**Highlights**

- BQ.1, BQ.1.1, XBB, and XBB.1 are the most resistant SARS-CoV-2 variants to date
- Serum neutralization was markedly reduced, including with the bivalent booster
- All clinical monoclonal antibodies were rendered inactive against these variants
- The ACE2 affinity of these variants were similar to their parental strains

Table S1

Sample ID	Vaccine type and infected strain	Days post-vaccination or *infection	Documented COVID-19	Age	Gender
Journal Pre-proof					
Q2	BNT162b2/BNT162b2/BNT162b2	30	No	68	Male
Q3	BNT162b2/BNT162b2/BNT162b2	14	No	64	Female
Q4	BNT162b2/BNT162b2/BNT162b2	34	No	55	Male
Q5	BNT162b2/BNT162b2/BNT162b2	34	No	45	Male
Q6	BNT162b2/BNT162b2/BNT162b2	15	No	50	Female
Q7	BNT162b2/BNT162b2/BNT162b2	15	No	48	Female
Q8	BNT162b2/BNT162b2/BNT162b2	29	No	71	Male
Q9	BNT162b2/BNT162b2/BNT162b2	90	No	59	Male
Q10	BNT162b2/BNT162b2/BNT162b2	33	No	45	Male
Q11	BNT162b2/BNT162b2/BNT162b2	87	No	66	Female
Q12	BNT162b2/BNT162b2/BNT162b2	84	No	26	Male
Q13	mRNA-1273/mRNA-1273/mRNA-1273	23	No	28	Female
Q15	BNT162b2/BNT162b2/mRNA-1273	32	No	39	Male
4 shots WT					
UM-65	BNT162b2/BNT162b2/BNT162b2/BNT162b2	24	No	52	Female
UM-66	BNT162b2/BNT162b2/BNT162b2/BNT162b2	20	No	57	Female
UM-67	BNT162b2/BNT162b2/BNT162b2/BNT162b2	20	No	61	Female
UM-68	mRNA-1273/mRNA-1273/mRNA-1273/mRNA-1273	22	No	48	Female
UM-69	BNT162b2/BNT162b2/BNT162b2/BNT162b2	23	No	50	Female
UM-70	BNT162b2/BNT162b2/BNT162b2/BNT162b2	22	No	50	Female
UM-71	BNT162b2/BNT162b2/BNT162b2/BNT162b2	20	No	58	Female
UM-72	BNT162b2/BNT162b2/BNT162b2/BNT162b2	26	No	56	Female
UM-73	BNT162b2/BNT162b2/BNT162b2/BNT162b2	29	No	63	Female
UM-74	BNT162b2/BNT162b2/BNT162b2/BNT162b2	25	No	58	Female
UM-75	BNT162b2/BNT162b2/BNT162b2/BNT162b2	21	No	62	Male
UM-76	BNT162b2/BNT162b2/BNT162b2/BNT162b2	26	No	54	Female
UM-77	BNT162b2/BNT162b2/BNT162b2/BNT162b2	23	No	53	Male
UM-78	BNT162b2/BNT162b2/BNT162b2/BNT162b2	21	No	55	Female
UM-79	BNT162b2/BNT162b2/BNT162b2/BNT162b2	23	No	59	Female
UM-80	BNT162b2/BNT162b2/BNT162b2/BNT162b2	21	No	49	Female
UM-81	BNT162b2/BNT162b2/BNT162b2/BNT162b2	27	No	57	Female
UM-82	BNT162b2/BNT162b2/BNT162b2/BNT162b2	27	No	55	Female
Q97	BNT162b2/BNT162b2/BNT162b2/BNT162b2	36	No	53	Female
3 shots WT + bivalent					
UM-36	BNT162b2/BNT162b2/BNT162b2/Moderna Bivalent	24	No	38	Female
UM-37	BNT162b2/BNT162b2/BNT162b2/Moderna Bivalent	27	No	42	Female
UM-39	mRNA-1273//mRNA-1273/mRNA-1273/Moderna Bivalent	24	No	36	Male
UM-40	BNT162b2/BNT162b2/BNT162b2/Pfizer Bivalent	25	No	37	Female
UM-41	BNT162b2/BNT162b2/BNT162b2/Pfizer Bivalent	24	No	36	Male
UM-43	BNT162b2/BNT162b2/BNT162b2/Pfizer Bivalent	25	No	49	Female
UM-44	BNT162b2/BNT162b2/BNT162b2/Moderna Bivalent	25	No	37	Female
UM-47	BNT162b2/BNT162b2/BNT162b2/Pfizer Bivalent	26	No	45	Male
UM-48	BNT162b2/BNT162b2/mRNA-1273/Moderna Bivalent	26	No	43	Female
UM-51	mRNA-1273/mRNA-1273/mRNA-1273/Moderna Bivalent	29	No	32	Female
UM-52	BNT162b2/BNT162b2/BNT162b2/Pfizer Bivalent	23	No	43	Female
UM-53	BNT162b2/BNT162b2/BNT162b2/Pfizer Bivalent	26	No	43	Female
UM-54	BNT162b2/BNT162b2/mRNA-1273/Moderna Bivalent	29	No	38	Female
UM-55	BNT162b2/BNT162b2/BNT162b2/Moderna Bivalent	28	No	38	Female
UM-56	BNT162b2/BNT162b2/mRNA-1273/Moderna Bivalent	27	No	36	Female
UM-60	BNT162b2/BNT162b2/BNT162b2/Moderna Bivalent	30	No	24	Female
Q101	mRNA-1273/mRNA-1273/mRNA-1273/Moderna Bivalent	30	No	32	Female
Q102	BNT162b2/BNT162b2/mRNA-1273/Moderna Bivalent	23	No	39	Male
Q103	BNT162b2/BNT162b2/BNT162b2/Pfizer Bivalent	30	No	26	Female
Q104	mRNA-1273/mRNA-1273/mRNA-1273/Pfizer Bivalent	30	No	27	Female
Q105	BNT162b2/BNT162b2/BNT162b2/Pfizer Bivalent	23	No	23	Male
BA.2 breakthrough					
Q35	BNT162b2/BNT162b2/BA.2	*14	Yes	50	Female
Q36	BNT162b2/BNT162b2/BNT162b2/Ad26_COV2.S/BA.2	*22	Yes	69	Male
Q49	BNT162b2/BNT162b2/mRNA-1273/BA.2	*16	Yes	32	Male
Q50	mRNA-1273/mRNA-1273/mRNA-1273/BA.2	*14	Yes	34	Male
Q51	BNT162b2/BNT162b2/mRNA-1273/BA.2	*19	Yes	33	Female
Q52	BNT162b2/BNT162b2/mRNA-1273/BA.2	*18	Yes	29	Female
Q98	BNT162b2/BNT162b2/BA.2	*122	Yes	22	Male
Q99	mRNA-1273/mRNA-1273/BA.2	*164	Yes	30	Female
Q100	BNT162b2/BNT162b2/BA.2	*94	Yes	30	Female
A7	BNT162b2/BNT162b2/mRNA-1273/BA.2	*30	Yes	59	Female
A9	BNT162b2/BNT162b2/BNT162b2/BA.2	*29	Yes	39	Female
A11	BNT162b2/BNT162b2/BNT162b2/BA.2	*18	Yes	45	Female
A12	BNT162b2/BNT162b2/BNT162b2/BNT162b2/BA.2	*31	Yes	59	Female
A13	BNT162b2/BNT162b2/BNT162b2/BNT162b2/BA.2	*25	Yes	39	Male
BA.4/5 breakthrough					
Q71	mRNA-1273/mRNA-1273/BNT162b2/BA.5.2.1	*29	Yes	29	Female
Q77	BNT162b2/BNT162b2/BNT162b2/BA.5	*22	Yes	61	Female
Q79	mRNA-1273/mRNA-1273/mRNA-1273/BA.5	*15	Yes	28	Female
Q80	mRNA-1273/mRNA-1273/mRNA-1273/BA.5	*21	Yes	24	Female
Q81	BNT162b2/BNT162b2/BNT162b2/BA.5	*75	Yes	35	Female
Q82	BNT162b2/BNT162b2/mRNA-1273/BA.5	*63	Yes	46	Female
Q83	BNT162b2/BNT162b2/BNT162b2/BA.5	*28	Yes	55	Male
Q84	BNT162b2/BNT162b2/BNT162b2/BA.5	*17	Yes	57	Female
UM-85	BNT162b2/BNT162b2/BNT162b2/BA.5	*29	Yes	44	Female
UM-86	BNT162b2/BNT162b2/mRNA-1273/BA.5	*29	Yes	36	Female
UM-87	BNT162b2/BNT162b2/BNT162b2/BNT162b2/BA.5	*31	Yes	54	Female
UM-88	BNT162b2/BNT162b2/BNT162b2/BNT162b2/BA.5	*28	Yes	69	Male
UM-89	BNT162b2/BNT162b2/BNT162b2/BNT162b2/BA.5	*42	Yes	44	Male
UM-90	BNT162b2/BNT162b2/BNT162b2/BNT162b2/BA.5	*28	Yes	41	Female
UM-91	BNT162b2/BNT162b2/BNT162b2/BNT162b2/BA.5	*28	Yes	44	Female
UM-92	BNT162b2/BNT162b2/BNT162b2/BNT162b2/BA.5	*31	Yes	29	Female
UM-93	BNT162b2/BNT162b2/BNT162b2/BNT162b2/BA.5	*29	Yes	48	Female
UM-94	BNT162b2/BNT162b2/BNT162b2/BNT162b2/BA.5	*29	Yes	49	Female
UM-95	BNT162b2/BNT162b2/mRNA-1273/BNT162b2/BA.5	*28	Yes	37	Female
UM-96	BNT162b2/BNT162b2/BNT162b2/BNT162b2/BA.5	*33	Yes	58	Female